

RSC Advances



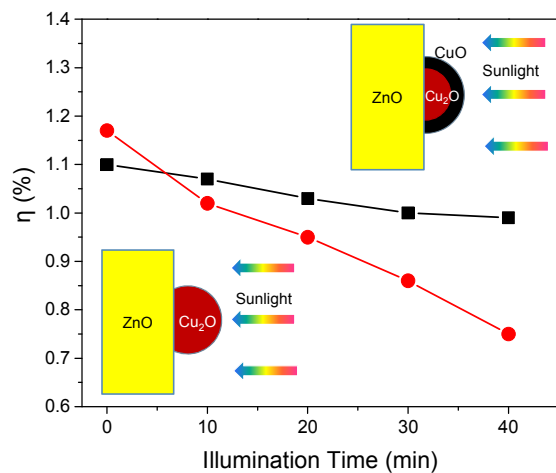
This is an *Accepted Manuscript*, which has been through the Royal Society of Chemistry peer review process and has been accepted for publication.

Accepted Manuscripts are published online shortly after acceptance, before technical editing, formatting and proof reading. Using this free service, authors can make their results available to the community, in citable form, before we publish the edited article. This *Accepted Manuscript* will be replaced by the edited, formatted and paginated article as soon as this is available.

You can find more information about *Accepted Manuscripts* in the [Information for Authors](#).

Please note that technical editing may introduce minor changes to the text and/or graphics, which may alter content. The journal's standard [Terms & Conditions](#) and the [Ethical guidelines](#) still apply. In no event shall the Royal Society of Chemistry be held responsible for any errors or omissions in this *Accepted Manuscript* or any consequences arising from the use of any information it contains.

$\text{Cu}_2\text{O}/\text{ZnO}$ hetero-nanorod arrays were successfully fabricated by a facile hydrothermal method followed a chemical bath deposition process. Also, a protective CuO layer on the Cu_2O quantum dots is prepared by simply heat-treating the heterostructure in air, which enhances the photovoltaic stability.



Chemical Bath Deposition of Cu₂O Quantum Dots onto ZnO Nanorod Arrays for Application in Photovoltaic Devices

Cite this: DOI: 10.1039/x0xx00000x

Xinwei Zou,^{ab} Huiqing Fan,^{*a} Yuming Tian,^b Mingang Zhang^b and Xiaoyan Yan^b

Received 00th January 2012,
Accepted 00th January 2012

DOI: 10.1039/x0xx00000x

www.rsc.org/

Cu₂O quantum dots (QDs) decorated ZnO nanorod arrays (ZNAs) were fabricated by a facile hydrothermal method following a chemical bath deposition (CBD) process. The surface morphology, crystal structure and photovoltaic behaviors of the heterostructure films were investigated. The results indicate that the Cu₂O QDs decorated on the ZNAs can be as good light absorber improving the visible spectral absorption, as well as the photo-induced electrons can easily transfer to ZnO, leading to an increase in the photovoltaic performance. When the CBD cycle taken for 10, an optimal photovoltaic performance could be obtained under the simulated sunlight illumination (AM 1.5G, 100 mW/cm²) with a photocurrent of 3.21 mA/cm², an open circuit photovoltage of 0.65 V and a conversion efficiency of 1.17%. Also, for improving the photovoltaic stability, a protective layer was prepared on the Cu₂O QDs by a simple process of heat treatment in ambient air at 100 °C for 2h. The results demonstrate that the passive CuO layer could be an effective protective layer for increasing the photovoltaic stability.

1. Introduction

At present silicon-based solar cells dominate the market of photovoltaics, but the silicon purification process is energy-intensive and very costly. So it is important to develop low cost, efficient and reliable photovoltaic materials for managing the growing global energy demand and reducing greenhouse gas emissions.¹ Metal oxides are considered to be potentially interesting candidates in this respect since the range of electronic and optical properties they support is truly exceptional.² Over the past ten years and more, ZnO have been deeply studied and widely used in various fields, such as light emitting diodes, photocatalysts, gas sensors, solar cells, and field emission devices, because it is photostable, nontoxic, low-cost and various morphologies readily available.^{3,4} However, a major drawback of ZnO is it can only absorb a small portion (~5%) of solar spectrum in the ultraviolet region because of its wide band gap of ~3.2 eV ($\lambda = 380$ nm).^{5,6} For extending the absorption range to the visible light region, various approaches have been utilized, including doping transition-metal ions into ZnO or sensitizing ZnO with a dye or another low band gap semiconductor.^{7,8} In the sensitization system, ZnO acts as an electron transporter for its high electron mobility and the dye or low band gap semiconductor acts as a light harvester for their wide photo-absorption region. Compared with other methods, sensitization systems have received more interest because of

their synergetic effects which not only extends the absorption range to visible light region but also decreases the probability of charge recombination under irradiation. To date, lots of semiconductors have been used as sensitizers for widening the absorption range, such as CdSe, CdS, PbS, WO₃ and Cu₂O etc.^{9,10} Among these materials, Cu₂O is of interest on account of its many advantages of narrow band gap of approximately 2.1 eV, non-toxicity, low cost and abundance of its starting material, i.e. copper. Hence, Cu₂O/ZnO heterostructure should be a promising material structure which can not only lead to a functional integration of the properties of both the Cu₂O and ZnO but also to novel interface effects and phenomena.¹¹ Until now many photovoltaic devices based on a Cu₂O/ZnO hetero-junction have been reported.¹²⁻¹⁴ While to synthesize these devices often needs expensive equipment (e. g. high temperature equipment, vacuum equipment and laser equipment). Aqueous method, such as hydrothermal growth, electrodeposition and chemical bath deposition, seems a promising method for preparing definitely low cost solar cells because it is simple and inexpensive and does not require complicated equipment. Chemical bath deposition (CBD) has been successfully employed to deposit quantum dots of metal chalcogenide, metal oxide and metal sulfide on ZnO or TiO₂ nanostructures.¹⁵⁻¹⁷ Moreover, control can be exercised on the morphology of the deposits by adjusting the precursor concentration, growth temperature and time or by using

templates and surfactants.¹⁸⁻²⁰ For example, High density perpendicularly orientated ZnO rod arrays have been obtained by using nanostructured thin films as seeding layers.²¹ Cu₂O nanorod thin films have been successfully grown on FTO glass substrate by using CBD technique with the assistance of CTAB.²²

Herein, we report synthesis of the hetero-nanostructure films comprising of ZnO nanorod arrays (ZNAs) decorated with Cu₂O QDs on the indium-doped tin oxide (ITO) glass substrates by a hydrothermal method following a CBD process. Also, a CuO passive layer is fabricated on the Cu₂O QDs as a protective layer by heat treatment. The detailed synthesis process and characterization of such films are expounded. The effects of the Cu₂O QDs amount and CuO layer on the photoelectrochemical properties of the resultant cells are investigated. Through extensive experimentation, we found that Cu₂O QDs could be an effective visible light sensitizer for ZNAs, which demonstrates that Cu₂O/ZnO hetero-nanorod arrays (Cu₂O QDs decorated ZNAs) can be used as a promising photoelectrode. In addition, the thin layer of CuO on Cu₂O QDs can be an effective protecting layer inhibiting the Cu₂O degradation in the photovoltaic process.

2. Experimental details

2.1. Preparation of Cu₂O/ZnO hetero-nanorod arrays

Firstly, vertically aligned pure ZNAs were prepared on transparent ITO/glass substrates (15 Ω/square) by a facile hydrothermal method reported previously.²³ In brief, a ZnO seed layer (ca. 10 nm) coat was prepared on the ITO glass substrate (ca. 15 mm × 25 mm) by spin coat method with a zinc oxide colloid (4.15 g zinc acetate dihydrate and 1.16 g monoethanolamine in 50 ml ethanol). Then the substrate with a seed coat was vertically immersed in a 40 ml equimolar aqueous solution of zinc nitrate and hexamethylenetetramine with a concentration of 0.10 M in a Teflon kettle and heated on a hot plate at 148 °C for 3 h.

Then, Cu₂O QDs were deposited on the ZNAs through a CBD process. The typical CBD process involved dipping the ZNAs into a colorless mixed aqueous solution of 20 ml 1.0 M CuSO₄ and 80 ml 1.0 M Na₂S₂O₃ (Solution I) for 2 s at room temperature, rinsing it with DI water, and then dipping it into a 0.5M NaOH aqueous solution (Solution II) for another 2 s at 70 °C, and rinsing it again with water. The two-step dipping procedure is considered as one CBD cycle. The incorporated amount of Cu₂O can be increased by repeating the assembly cycle.

2.2. Characterization

The morphology of the heterostructure nanorod arrays was characterized by scanning electron microscopy (SEM, Supra 55, Zeiss, Oberkochen, Germany) and transmission electron microscopy (TEM, Tecnai F30 G2, FEI, Hillsboro, OR, USA). X-ray diffractometer (XRD, X'Pert MPD, Philips, Amsterdam, The Netherlands), Energy-dispersive X-ray spectrometer (EDS, INCA Xstream-2, Oxford, Abingdon, Oxfordshire, UK) attached to the SEM, and X-ray photoelectron spectrometer (XPS, K-Alpha, Thermo Scientific, Atlanta, GA, USA) were used to characterize the phase and chemical composition of the heterostructure nanorod arrays. Ultraviolet-visible spectra of

the heterostructure films were recorded by a spectrophotometer (UV-3150, Shimadzu, Tokyo, Japan).

2.3. Photovoltaic performance and EIS measurements

The sandwich cells were assembled for investigating the photovoltaic performance of the heterostructure nanorod arrays. The Pt counter-electrode was prepared by dripping a drop of 5 mM H₂PtCl₆ isopropyl alcohol solution onto an ITO glass substrate (ca. 15mm×25mm), followed by heating at 385 °C for 30 min. The heterostructure nanorod arrays used as photoanode and the counter-electrode were cohered together by a Surlyn film. The space between the two electrodes was controlled at ~3 mm. The electrolyte comprised of 0.2 M Na₂SO₄ and 0.1 M NaCH₃COO (pH 7) according to a previous report.²⁴ A Keithley 2410 source meter was used to measure photocurrent at a scan rate of 10mV/s. Sunlight was simulated with a 500W xenon lamp (Spectra Physics). The light intensity was adjusted to 1 sun condition (AM 1.5G, 100mW/cm²) using a NREL-certified Si reference cell. The effective area of the cell was 0.5 cm². The incident photon-to-electron conversion efficiency (IPCE) under monochromated light (350-800 nm) was measured by an IPCE system (QTest Station 1000, CrownTech, Macungie, PA, USA). A 150 W tungsten halogen lamp was used as the light source to generate a monochromatic beam. A silicon solar cell was used as the standard during calibration. The electrochemical impedance spectroscopy (EIS) measurements were carried out on an electrochemical workstation (CHI600E, CH Instruments, Shanghai, China) under the same simulated sunlight illumination. The impedance spectra were recorded with the help of CHI 13.07 software under an AC perturbation signal of 10 mV over the frequency range of 1 MHz to 0.01 Hz at 0.3 V in the dark.

3. Results and discussion

3.1. SEM and EDS analysis

Fig. 1a shows the SEM image of the pure ZNAs grown on an ITO/glass substrate by the hydrothermal method. It can be appreciated that all of the nanorods show hexagonal-rod morphology with smooth surface and planar top ends which results from their wurtzite structure.²³ The majority of nanorods are vertically oriented to the substrate plane. Moreover, the axial direction is aligned with the c-axis of the hexagonal ZnO crystal structure.⁸ The nanorods have a mean diameter of 207 nm which is obtained by measuring 30 individual nanorods and has a standard deviation of 66. Fig. 1b, c, d and e shows the SEM images of the heterostructure nanorod arrays obtained at different CBD cycles. Insets in Fig. 1b, c, d and e are the corresponding larger magnification images of the different heterostructure nanorod arrays. It can be clearly seen that the side of the ZnO nanorods is rather rough and possesses uniform nanoparticles. Also we can estimate the particle size of the Cu₂O quantum dot obtained at different CBD cycles is 11 nm (2 cycles), 28 nm (5 cycles), 55 nm (10 cycles) and 120 nm (20 cycles), respectively. Comparing these SEM images of Fig. 1b, c, d and e, it can be found that as the CBD cycle increases, the amount of the nanoparticles increases and the nanorod shape becomes a little round from hexagonal. Fig. 1f shows the typical energy-dispersive spectrum (EDS) taken on the nanoparticles. Only the elements of O, Zn and Cu can be observed, which indicates that these nanoparticles should be

copper oxide. The atomic ratio of Cu, Zn and O is estimated to be 7.02%, 49.39% and 43.59%, respectively. It cannot imply that the nanoparticles are comprised of only Cu_2O . Maybe it also contains some CuO . So a further characterization is needed.

3.2. Phase and chemical composition

The phase and chemical composition of the heterostructure nanorod arrays were further examined by X-ray diffractometer and energy dispersive X-ray spectrometer. Fig. 2A shows the X-ray diffractogram of the heterostructure nanorod arrays obtained at different CBD cycles. As for the pure ZNAs grown on ITO substrates (0 cycles), all the diffraction peaks agree well with the hexagonal zincite phase (JCPDS 36-1451). The enhanced (0 0 2) diffraction peak at 2θ of 34.42 also indicates the as-prepared ZNAs are oriented with respect to the substrate. As for the heterostructure nanorod arrays obtained at CBD

cycles of 10 and 20 (d and e patterns in Fig. 2A), besides the ZnO diffraction peaks, the Cu_2O (111), (200), (220) and (311) peaks are emerged at 2θ of 36.50, 42.38, 61.50 and 73.69, respectively, which agree well with the crystal planes of cubic Cu_2O (JCPDS 65-3288). The Cu_2O (111) peak ($2\theta = 36.50$) is very close to the ZnO (101) peak ($2\theta = 36.25$), and they are overlapped in the pattern. Comparing with ZnO peaks, the Cu_2O peaks are very weak, which revealing that the Cu_2O deposited onto ZnO are of very small size or amount.²⁵ As for the heterostructure nanorod arrays obtained at CBD cycles of 2 and 5 (b and c patterns in Fig. 2A), no evident Cu_2O diffraction peaks are observed. There may be two reasons caused for the absence of Cu_2O peaks, the first one may be that only few QDs are attached to the ZnO nanorods, the other may be that the Cu_2O QDs are highly dispersed on ZnO surface.¹⁷

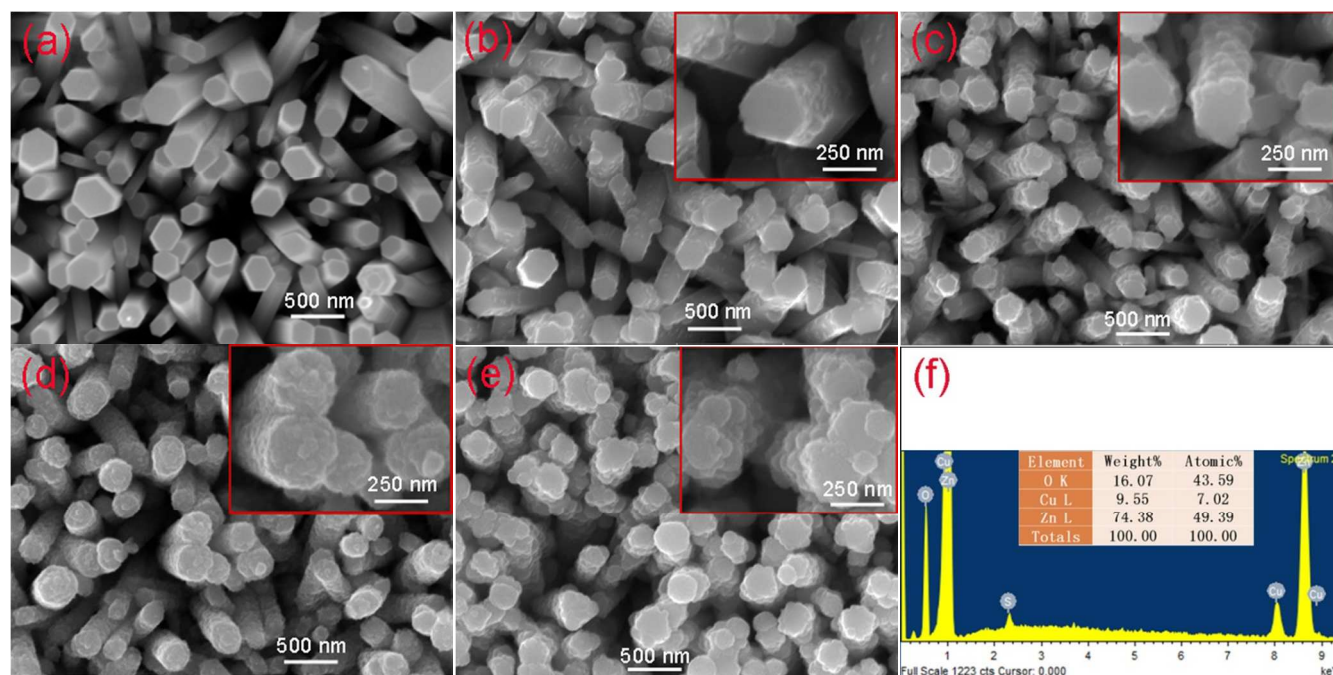


Fig. 1 SEM image of pure ZNAs (a) and $\text{Cu}_2\text{O}/\text{ZnO}$ hetero-nanorod arrays obtained at different CBD cycles: 2 cycles (b), 5 cycles (c), 10 cycles (d) and 20 cycles (e). The typical EDS of the $\text{Cu}_2\text{O}/\text{ZnO}$ hetero-nanorod arrays (f).

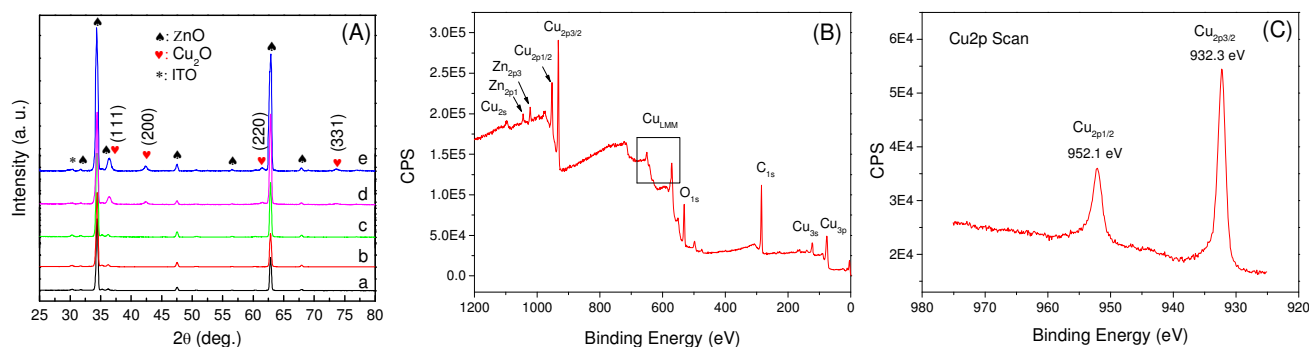


Fig. 2 (A) X-ray diffractogram of the $\text{Cu}_2\text{O}/\text{ZnO}$ hetero-nanorod arrays of different CBD cycles: a – 0 cycles, b – 2 cycles, c – 5 cycles, d – 10 cycles and e – 20 cycles. (B) XPS survey spectrum of $\text{Cu}_2\text{O}/\text{ZnO}$ hetero-nanorod arrays. (C) The high resolution XPS Cu 2p scan spectrum of the $\text{Cu}_2\text{O}/\text{ZnO}$ hetero-nanorod arrays.

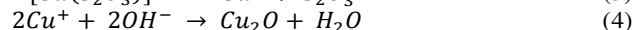
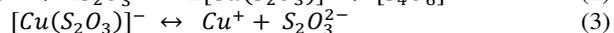
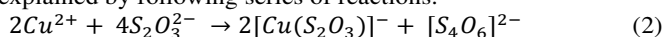
PAPER

Taken together, from Fig. 2A we can see that the intensities of the Cu_2O characteristic peaks increase with the increase in CBD cycles, suggesting the increased amount of the Cu_2O QDs. Then X-ray photoelectron spectroscopy (XPS) was employed to confirm the presence of heterostructure nanorod arrays (Fig. 2B and C). The whole survey of the heterostructure nanorod arrays surface presents all the elements detected, as shown in Fig. 2B. Since only C (from atmosphere), O, Zn and Cu were detected, it suggests that only copper oxide or zinc oxide was formed on the surface, this agrees well with the EDS result. In the Cu 2p spectrum (Fig. 2C), there are only two peaks located at 932.3 eV (Cu 2p_{3/2}) and 952.1 eV (Cu 2p_{1/2}) for the heterostructure nanorod arrays, indicating the existence of Cu^+ .²⁵ Furthermore, the Cu 2p_{1/2} and Cu 2p_{3/2} satellite peaks for Cu^{2+} were not observed, which provides powerful evidence for the successful coating of only Cu_2O on the surface of ZnO nanorods.²⁶

3.3. TEM images and Cu_2O growth mechanism

The bright-field transmission electron microscopy (TEM) image in Fig. 3a is a representative ZnO nanorod decorated with an ensemble of Cu_2O QDs. The grey spots on the surface of the nanorod should be Cu_2O QDs, the size is about 5~7 nm in diameter. These tiny Cu_2O QDs can aggregate forming the larger nanoparticles as seen in SEM images. Fig. 3b shows a high-resolution transmission electron microscopy (HRTEM) image of the circle area in Fig. 3a. The larger crystallite appearing in the left region of the image is identified to be ZnO. The lattice spacing measured for this crystalline plane is 5.21 Å, corresponding to the (001) plane of hexagonal ZnO and the growth direction of the nanorods is dominantly [001]. The attached QDs appear as randomly oriented crossed fringe patterns on the edge of the nanorod. And the observed lattice fringe of 2.45 Å is corresponding to the (1 1 1) crystal plane of the cubic phase of Cu_2O (JCPDS 65-3288).

The formation of Cu_2O QDs on ZnO nanorod via CBD can be explained by following series of reactions.^{22, 27, 28}



During the CBD process, in the colorless Solution I the copper thiosulfate complex can be formed from eqn (2), in which CuSO_4 and $\text{Na}_2\text{S}_2\text{O}_3$ are introduced as precursor of Cu_2O and reducing agent, respectively. Cu^+ cations are formed by dissociation equilibrium (eqn 3). When the as-drawn ZNAs from Solution I is immersed in the Solution II (NaOH hot solution), the adherent Cu^+ cations react with OH^- anions to form Cu_2O QDs on the surface of ZNAs and the eqn (4) chemical reaction occurs. As the CBD cycle increases, the amount of Cu_2O QDs grows big gradually.

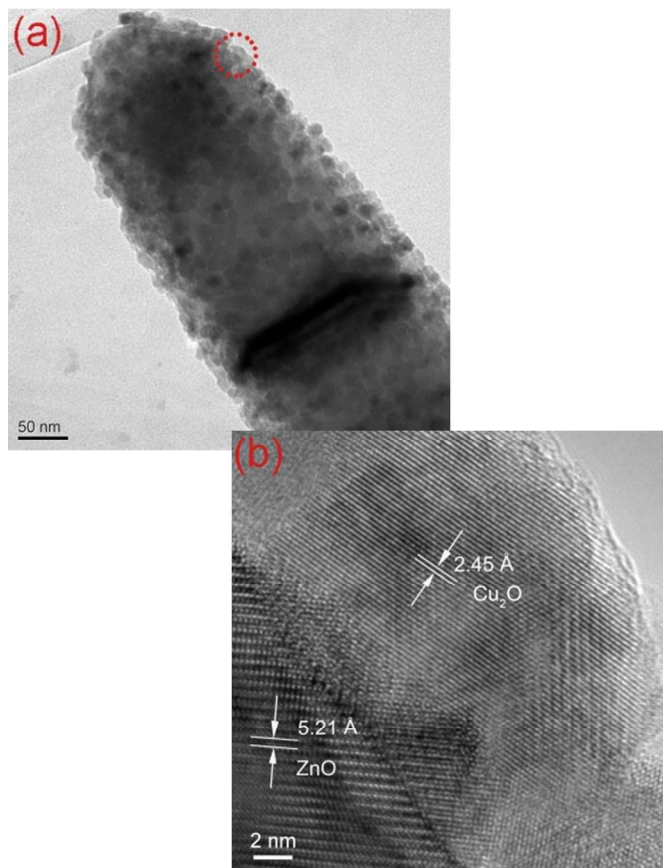


Fig. 3 Bright-field TEM (a) and HRTEM (b) images of the representative $\text{Cu}_2\text{O}/\text{ZnO}$ hetero-nanorod

3.4. UV-vis absorption spectroscopy

Fig. 4 shows the UV-vis absorption spectra of ZNAs and $\text{Cu}_2\text{O}/\text{ZnO}$ hetero-nanorod arrays of different CBD cycles. The maximum absorbance peak of the ZNAs occurs at around 380nm and almost has no absorbance for visible-light due to its large energy gap (~3.2 eV). Compared with the ZNAs, the $\text{Cu}_2\text{O}/\text{ZnO}$ hetero-nanorod arrays show significantly red-shift of the peak maxima at 550nm and exhibit broad absorption bands from 200 to 550 nm, indicating the effective photo-absorption ability for the heterostructure. In addition, the absorbance of the spectra increases as the CBD cycles. Furthermore, the absorption edge shifts slightly to red with the increase of CBD cycles, indicating the growth of the Cu_2O particles. The band gap for the Cu_2O bulk is 2.2 eV at room temperature. However, when the particle size is reduced to the quantum-size, the number of atoms will be significantly decreased, causing a larger interval of the electron energy level.

Hence, the electrons no longer possess continuous energy bands. The electronic energy level will change from quasi-continuous phase to split phase and the band gap will become wider, leading to the blue shift of the absorption.^{17, 29} Therefore, it is easy to understand the slight red shift of the absorption edge when the CBD cycles are increased.

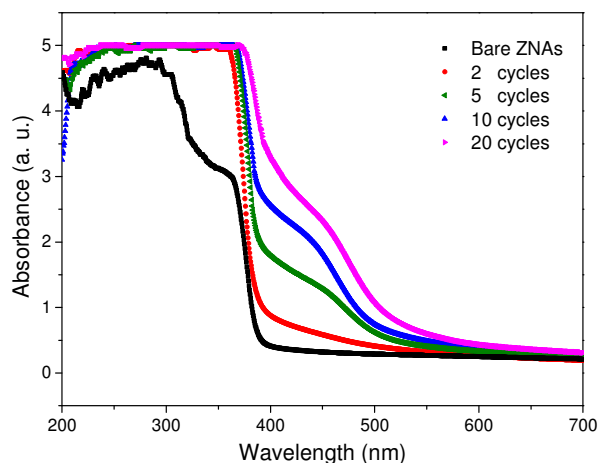


Fig. 4 UV-vis absorption spectra of pure ZnOs and the Cu₂O/ZnO hetero-nanorod arrays of different CBD cycles.

3.5. Photovoltaic performance

Fig. 5 shows the characteristics of the photocurrent density versus applied voltage (*J-V* curve) of the Cu₂O/ZnO heterostructure nanorod arrays based solar cells under simulated sunlight. Table 1 lists the photovoltaic parameters obtained from the *J-V* curves, including short circuit current (J_{sc}), open circuit potential (V_{oc}), fill factor (FF), and the total power conversion efficiency (η). As for the bare ZnOs photoelectrode, the photovoltaic performance almost can be neglected due to the infinitesimally small J_{sc} (only 0.20 mA/cm²). As for the Cu₂O/ZnO heterostructure nanorod arrays with CBD 10 cycles electrode, J_{sc} is about 3.21 mA/cm², which is more than 16 times higher than that of the bare ZnOs photoelectrode. The optimum power conversion efficiency is 1.17% for the Cu₂O/ZnO heterostructure photoelectrodes. The comparison between the photovoltaic behavior of bare ZnOs and Cu₂O/ZnO heterostructure photoelectrodes confirms the superior performance of producing higher photocurrents and power conversion efficiencies for the latter over those of the former. The enhanced photovoltaic property can be ascribed to the following probable reasons: Firstly, the extension of absorption spectrum into the visible region by Cu₂O/ZnO heterostructure photoelectrodes. Compared with bare ZnOs photoelectrode, these photoelectrodes have an intense absorption in the visible region, greatly raised the utilization rate of the solar energy. Secondly, the reduction in recombination rate of photo-induced electron-hole pairs because of the heterojunction structure. As shown in Fig 6, the conduction band position of Cu₂O is higher than that of ZnO, once incident photons are absorbed by the Cu₂O QDs, photo-

generated electrons in the conduction band of Cu₂O will quickly transfer into that of the ZnO to decrease its energy level. In this way, photo-generated electron-hole pairs are separated quickly and transported in their respective phases to the opposing electrodes, leading to enhance photovoltaic efficient.

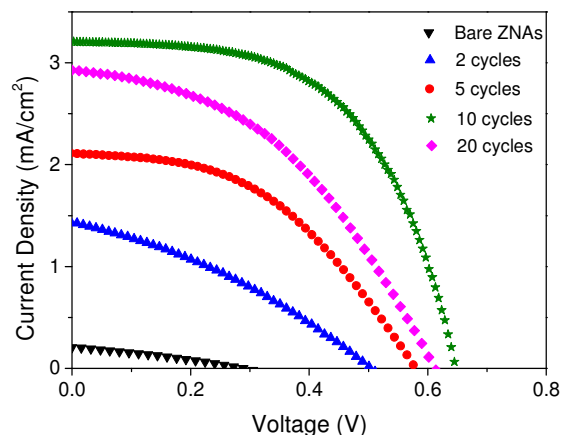


Fig. 5 Photocurrent density versus applied voltage curves for the solar cells based on Cu₂O/ZnO hetero-nanorod arrays of different CBD cycles

Furthermore, it can be easily found that for a certain applied potential, all the photovoltaic parameters increase sharply as CBD cycles in the early stage, indicating that a higher incorporated amount of Cu₂O can induce a higher power output. However, the photovoltaic parameters are found to somewhat decrease when the CBD cycles are increased to 20 cycles. This phenomenon may be attributed to that more CBD cycles would cause conglomeration and growth of the Cu₂O crystal nucleus, and the oversized Cu₂O particles will lose the dominance as QDs (large QD extinction coefficients and generating multiple electron-hole pairs), and moreover, excess Cu₂O nanoparticles can act as potential barrier for charge transfer.¹⁷ Fig. 7 shows the IPCE value of the different Cu₂O/ZnO heterostructure nanorod arrays based solar cells as a function of wavelength. The IPCE curve indicates the light response of the photovoltaic device, which is directly related to the photocurrent density. The IPCE presents a similar threshold to UV-vis absorbance. The quantum efficiencies of the different Cu₂O/ZnO heterostructure photoanodes vary in the range of 400~700 nm corresponding to the effect of the Cu₂O QDs CBD cycles. The results are in accordance with the *J-V* curves.

It is noted that the power conversion efficiencies measured for the Cu₂O/ZnO QDs sensitized solar cell here are less than the highest value of a solid state heterojunction solar cell previously reported in the literature (5.38%).¹⁴ This can be attributed, at least in part, to the high density of interface states at the Cu₂O/ZnO heterojunction resulting from the aqueous synthesis, which facilitate unwanted charge recombination.³⁰ Another reason presumably is due to the inappropriate electrolyte.

Table 1 Parameters obtained from the J-V curves of the solar cells based on different photoelectrodes.

Electrode	J_{sc} (mA/cm ²)	V_{oc} (V)	FF (%)	η (%)
0 cycle	0.20	0.29	30.67	0.01
2 cycles	1.43	0.50	33.36	0.24
5 cycles	2.11	0.58	45.62	0.56
10 cycles	3.21	0.65	56.46	1.17
20 cycles	2.93	0.61	42.79	0.77

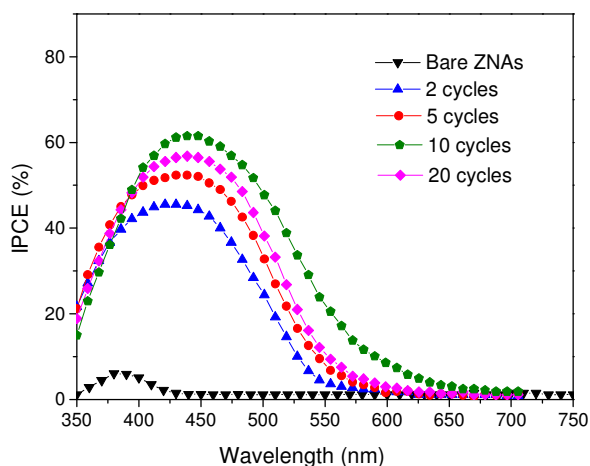


Fig. 7 IPCE curves of the solar cells based on Cu₂O/ZnO hetero-nanorod arrays with different CBD cycles

3.6. EIS spectra

To further understand the effect of the Cu₂O QDs on the charge transfer kinetics and internal resistance of the Cu₂O QDs sensitized solar cells, EIS measurements were conducted and the results are shown in Fig. 8. As can be seen from the Nyquist plots, all the plots show two partially overlapped semicircles in the high-to-medium frequency region and a large arc in the low frequency region. The corresponding equivalent circuit for this cell system is depicted in the inset (I) of Fig. 8.³¹ The first small semicircle in the high-frequency range can be assigned to the charge transfer resistance (R_{CE}) and double-layer capacitance (C_{CE}) at the CE/electrolyte interface.^{32, 33} The second large semicircle in the medium frequency region is due to the charge transfer resistance of the recombination process (R_r) and the interfacial capacitance (C_{μ}) at the ZnO/Cu₂O/electrolyte interface.³³ The right larger arc appearing in the low frequency region is attributed to the Warburg impedance (Z_d) of the redox couple in the electrolyte.³⁴ The R_r , C_{μ} and calculated electron lifetime (τ_n) of the different cells determined from EIS analysis fitted results are listed in Table 2. We can find that the R_r of the different cells increases as the CBD cycles.

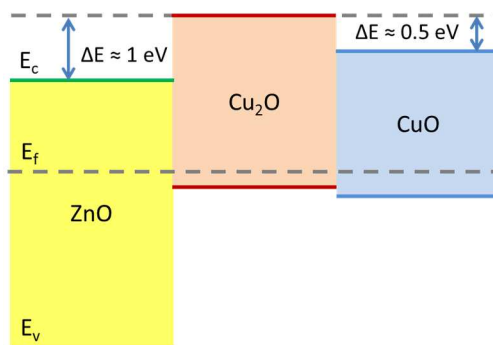


Fig. 6 Energy band alignment diagram of the ZnO/Cu₂O/CuO heterojunction

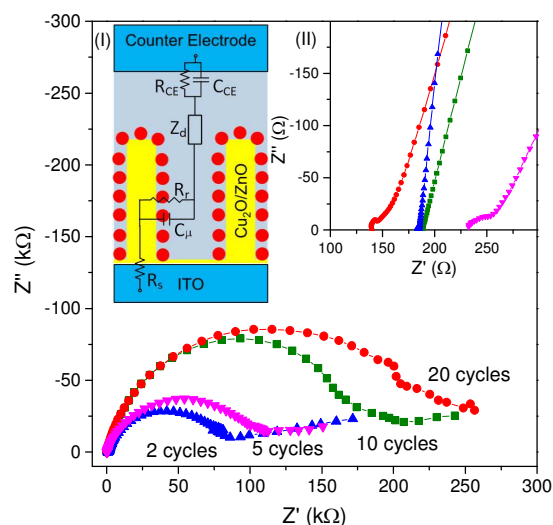


Fig. 8 Nyquist plots of the cells based on Cu₂O/ZnO hetero-nanorod arrays of different CBD cycles. Insets are the equivalent circuit used to fitting the Nyquist plots (I) and the magnified plots of the first semicircle (II)

The larger value of R_r implies the retarded backward reaction of injected electron transfer at the ZnO/Cu₂O/electrolyte interface, i.e., reduced interfacial recombination resulting in high efficiency.³⁵ As the poor loading of QDs would cause the direct exposure of ZnO to the electrolyte, which might be responsible for the comparative low R_r for the photoanode with less CBD cycles. The C_{μ} is related to the density of states and the surface recombination sites. An increase in the capacitance could indicate passivation of the surface recombination sites.³⁶ Therefore, larger C_{μ} means more number of photo-excited electrons can be transferred into the conduction band of ZnO indicating the reduction of charge recombination. As shown in Table 2, the value of C_{μ} increases as the CBD cycles at beginning then decreases and the photoanode with 10 CBD cycles shows the largest C_{μ} value. This variation tendency in C_{μ} is consistent with the η results presented in Table 1. The electron lifetime (τ_n) is another parameter can reflect the charge recombination rate and the electron-transfer rate, and it can be calculated from $\tau_n = R_r C_{\mu}$.^{16, 37} It can be seen that the photoanode with 10 CBD cycles has the largest electron

lifetime, which again indicates a reduced charge-transfer rate. In spite of the low charge-transfer resistance of the photoanode with CBD 10 cycles compared with that of the photoanode with CBD 20 cycles, the electron lifetime of the photoanode with CBD 10 cycles is larger than that of the photoanode with CBD 20 cycles, and this result is in good agreement with the larger C_{μ} value. As for the photoanode with CBD 20 cycles, the abundant Cu_2O QDs covered the total surface of the ZnO nanorods and some aggregated on the surface of the ZnO nanorods due to more CBD cycles. The larger aggregates could result in a longer transport path length for the photo-induced electron-hole pairs in the Cu_2O sensitizer before being separated and collected, and thus act as a potential barrier for charge transfer. So the charge recombination process in Cu_2O is enhanced.^{37, 38}

Table 2 Parameters obtained from the fitting results of the electrochemical impedance spectra.

Electrode	R_r (k Ω)	C_{μ} (μF)	τ_n (ms)
2 cycles	82.1	1.1	90.3
5 cycles	103.9	1.5	155.9
10 cycles	203.8	3.2	652.2
20 cycles	214.5	1.8	386.1

3.7. Effect of the CuO protective layer

According to the previous studies, we know that the stability of Cu_2O could be enhanced due to the fast charge transfer and blocking of anodic currents when paired with other oxide semiconductors such as ZnO or TiO_2 .^{8, 39} When the heterostructure photoanode is exposed under the weak monochromated light illumination, no significant dissolution or phase transformation of Cu_2O is happened. However, under intense illumination, Cu_2O is found to be no longer stable, even when it paired with other oxide semiconductors.²⁴ As shown in Fig. 9, the η of the cell based on the as-prepared $\text{Cu}_2\text{O}/\text{ZnO}$ heterostructure with CBD 10 cycles is decreased as the illumination time prolonged. It can be found that the η is decreased by as much as 36% after a 40 min illumination from 1.17% to 0.75%. Hence, there is a tremendous requirement to improve the photochemical stability of the $\text{Cu}_2\text{O}/\text{ZnO}$ heterostructure electrode.

As Thimsen and his co-workers reported, the Cu_2O photoelectrode could be highly stabled by depositing a protective layer of $\text{Al}/\text{ZnO}/\text{TiO}_2$ on the top of Cu_2O using atomic layer deposition (ALD).⁴⁰ The protective oxide layer can prevent the Cu_2O electrode from being in contact with the electrolyte without changing the energy band position. CuO is a relatively stable phase of copper oxide and thus could be used as an effective protection layer to minimize the degradation of Cu_2O under the illumination condition. Wang's group reported a two-step electrodeposition-anodization process to prepare a CuO nanowire mounted Cu_2O composite photoelectrode with improved stability.⁴¹ The presence of CuO can improve the charge separation of Cu_2O , which suppresses the redox reactions of Cu_2O .⁴²

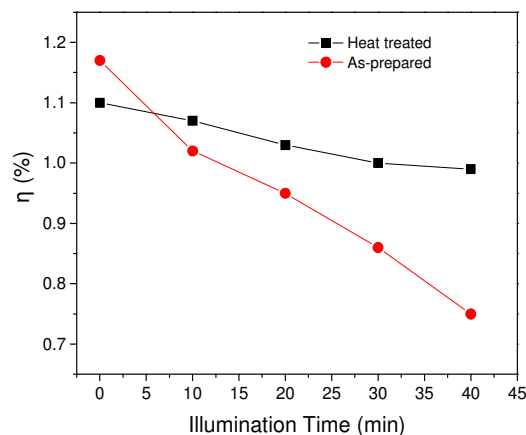


Fig. 9 Power conversion efficiencies (η) of the as-prepared and heat-treated photoelectrodes at different illumination time.

Here, as for our $\text{Cu}_2\text{O}/\text{ZnO}$ heterostructure photoelectrode, CuO coating layer has been fabricated on the Cu_2O QDs by a simply heat treatment process in ambient air at 100 °C for 2h. For a further characterization of the heat-treated $\text{Cu}_2\text{O}/\text{ZnO}$ photoelectrode, XRD, TEM and XPS analysis were carried out. The XRD and TEM results show no difference between the as-prepared and heat-treated $\text{Cu}_2\text{O}/\text{ZnO}$ heterostructure nanorod arrays photoelectrodes. This can be ascribed to the little amount of CuO formed on the surface of Cu_2O QDs. XPS is a powerful technique for the study of the surface elemental composition, chemical state and electronic state of the elements. Fig. 10 shows the Cu 2p XPS depth profile spectra of the heat-treated $\text{Cu}_2\text{O}/\text{ZnO}$ hetero-nanorod arrays of CBD 10 cycles. A clear difference in the shapes can be observed for the surface and underneath scan spectra, being in agreement with those previously reported and discussed in the literature for Cu^+ and Cu^{2+} species.^{26, 43} As for the Cu 2p spectrum obtained after an argon ion sputter etching process for 10 s (below spectrum in Fig. 10), it is well consistent with the spectrum in Fig 2C, only the binding energy peaks related to Cu 2p_{3/2} and Cu 2p_{1/2} of Cu_2O emerged. Thereby, it indicates the core of the QDs is still composed of Cu_2O . In the Cu 2p surface scan spectrum obtained before etching, there are two main peaks located at around 934.4 and 954.0 eV which are assigned to the binding energy of Cu 2p_{3/2} and Cu 2p_{1/2}, respectively. Meanwhile, we can find that the Cu 2p_{1/2} and 2p_{3/2} peaks are relatively broad, which seems to be influenced by the presence of other copper species. For acquiring a more precise knowledge about this, we fitted the peaks using a Gaussian/Lorentzian mixed function. From the peak-fit for the Cu 2p, we find two other small peaks (1 and 5) with binding energy of 932.5 and 952.8 eV, which are assigned to Cu 2p_{3/2} and Cu 2p_{1/2} of Cu_2O , respectively.^{41, 43} Moreover, there are a series of extra shake-up satellite peaks observed on a higher binding energy side, 940.6 (peak 3), 943.3 (peak 4) and 962.2 eV (peak 7) for Cu 2p_{3/2} and Cu 2p_{1/2} respectively, which can be ascribe to an unfilled Cu 3d⁹ shell and indicates the presence of CuO on the surface.^{42, 43}

Based on the above-described results that the strong XPS peaks of Cu^{2+} peaks and relatively low for peaks Cu^+ , it implies a protection layer of CuO formed on the top of Cu_2O . Because the sputtering time is very short, the CuO layer should be very thin. Although the layer of CuO is thin, the photoelectrochemical stability can be improved significantly.

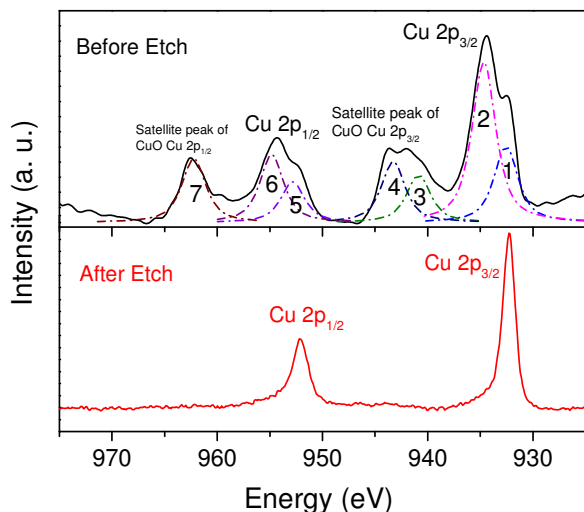


Fig. 10 Cu 2p XPS depth profile spectra of the heat-treated $\text{Cu}_2\text{O}/\text{ZnO}$ hetero-nanorod of CBD 10 cycles

As shown in Fig. 9, the η of the cell based on the heat-treated $\text{Cu}_2\text{O}/\text{ZnO}$ hetero-nanorod arrays of CBD 10 cycles is decreased from 1.10 to 0.99% after a 40 min illumination; it only decreases by 10%. The photoelectrochemical stability is increased obviously on the same condition. This result indicates that CuO can be as an effective protecting layer for the $\text{Cu}_2\text{O}/\text{ZnO}$ photoelectrodes enhancing the photoelectrochemical stability of the assembled solar cells. Compared with the as-prepared $\text{Cu}_2\text{O}/\text{ZnO}$ of CBD 10 cycles, the initial η is slightly decreased. As shown in Fig. 6, the conduction band of CuO is lower than that of Cu_2O . The photo-generated electrons in the conduction band of Cu_2O are apt to transfer into that of the CuO to decrease its energy level. This goes against the electron transfer to ZnO and increases the charge recombination, leading to decrease photovoltaic efficient.

4. Conclusions

The Cu_2O quantum dots can be successfully prepared on ZNAs forming the $\text{Cu}_2\text{O}/\text{ZnO}$ heterostructure system by the chemical bath deposition technique. It is a promising model system for photovoltaic, photoelectrochemical and photocatalytic applications since it comprises relatively inexpensive materials and can be fabricated at low energy intensity. In addition, it is capable to use a significant fraction of the solar spectrum. The Cu_2O quantum dots amount has an effect on the photovoltaic performance. Also, it is shown that the heat treatment promotes the photovoltaic stability of $\text{Cu}_2\text{O}/\text{ZnO}$ under simulated

sunlight illumination due to the CuO protective layer formed at the surface of Cu_2O inhibiting the corrosion process.

Acknowledgements

The work was supported by the National Natural Science Foundation (51172187), the SPDRF (20116102130002) and 111 Program (B08040) of MOE, and Xi'an Science and Technology Foundation (CX12174, XBCL-01-08), and Shaanxi Province Science Foundation (2013KW12-02), and the SKLP Foundation (KP201421), and the Fundamental Research Funds for the Central Universities (3102014JGY01004) of China.

Notes and references

^a State Key Laboratory of Solidification Processing, School of Materials Science and Engineering, Northwestern Polytechnical University, Xi'an 710072, PR China.

^b School of Materials Science and Engineering, Taiyuan University of Science and Technology, Taiyuan 030024, PR China.

*Corresponding author.

Tel.: + 86 29 88494463; Fax: + 86 29 88492642.

E-mail address: hqfan3@163.com

- 1 A. S. Zoofakar, R. A. Rani, A. J. Morfa, S. Balendhran, A. P. O'Mullane, S. Zhuiykov and K. Kalantar-zadeh, *J. Mater. Chem.*, 2012, 22, 21767.
- 2 M. Deo, S. Mujawar, O. Game, A. Yengantiwar, A. Banpurkar, S. Kulkarni, J. Jog and S. Ogale, *Nanoscale*, 2011, 3, 4706.
- 3 Y. Wang, S. Li, H. Shi and K. Yu, *Nanoscale*, 2012, 4, 7817.
- 4 J.-X. Sun, Y.-P. Yuan, L.-G. Qiu, X. Jiang, A.-J. Xie, Y.-H. Shen and J.-F. Zhu, *Dalton. Trans.*, 2012, 41, 6756.
- 5 X. Zhang, J. Qin, Y. Xue, P. Yu, B. Zhang, L. Wang and R. Liu, *Sci. Rep.*, 2014, 4.
- 6 S. S. Mali, H. Kim, P. S. Patil and C. K. Hong, *Dalton. Trans.*, 2013, 42, 16961.
- 7 Y. Wang, G. She, H. Xu, Y. Liu, L. Mu and W. Shi, *Mater. Lett.*, 2012, 67, 110.
- 8 X. W. Zou, H. Q. Fan, Y. M. Tian and S. J. Yan, *Crystengcomm*, 2014, 16, 1149.
- 9 W. Jia, H. L. Dong, J. F. Zhao, S. H. Dang, Z. X. Zhang, T. B. Li, X. G. Liu and B. S. Xu, *Appl. Phys. A-mater.*, 2012, 109, 751.
- 10 S. Balachandran and M. Swaminathan, *Dalton. Trans.*, 2013, 42, 5338.
- 11 M. Deo, D. Shinde, A. Yengantiwar, J. Jog, B. Hannover, X. Sauvage, M. More and S. Ogale, *J. Mater. Chem.*, 2012, 22, 17055.
- 12 T. Minami, Y. Nishi, T. Miyata and J.-i. Nomoto, *Applied Physics Express*, 2011, 4, 062301.
- 13 Y. Nishi, T. Miyata and T. Minami, *Journal of Vacuum Science & Technology A*, 2012, 30.
- 14 T. Minami, Y. Nishi and T. Miyata, *Applied Physics Express*, 2013, 6, 044101.
- 15 C.-H. Chang and Y.-L. Lee, *Appl. Phys. Lett.*, 2007, 91, 053503.
- 16 Y. Choi, M. Seol, W. Kim and K. Yong, *J. Phys. Chem. C*, 2014, 118, 5664.
- 17 H. Chen, W. Y. Fu, H. B. Yang, P. Sun, Y. Y. Zhang, L. R. Wang, W. Y. Zhao, X. M. Zhou, H. Zhao, Q. A. Jing, X. F. Qi and Y. X. Li, *Electrochim. Acta*, 2010, 56, 919.
- 18 A. M. Lockett, P. J. Thomas and P. O'Brien, *J. Phys. Chem. C*, 2012, 116, 8089.
- 19 G. Mu, R. V. Gudavarthy, E. A. Kulp and J. A. Switzer, *Chem. Mater.*, 2009, 21, 3960.
- 20 Q. Li, J. Bian, J. Sun, J. Wang, Y. Luo, K. Sun and D. Yu, *Appl. Surf. Sci.*, 2010, 256, 1698.
- 21 D. S. Boyle, K. Govender and P. O'Brien, *Chem. Commun.*, 2002, 7, 80.
- 22 A. A. Aref, L. Xiong, N. Yan, A. M. Abdulkarem and Y. Yu, *Mater. Chem. Phys.*, 2011, 127, 433.
- 23 X. W. Zou, H. Q. Fan, Y. M. Tian and S. J. Yan, *Mater. Lett.*, 2013, 107, 269.
- 24 L.-k. Tsui and G. Zangari, *Electrochim. Acta*, 2014, 128, 341.

- 25 S. Zhang, S. Zhang, F. Peng, H. Zhang, H. Liu and H. Zhao, *Electrochem. Commun.*, 2011, 13, 861.
- 26 J. Morales, L. Sánchez, F. Martín, J. R. Ramos-Barrado and M. Sánchez, *Thin Solid Films*, 2005, 474, 133.
- 27 Q. Pan, M. Wang and Z. Wang, *Electrochem. Solid State Lett.*, 2009, 12, A50.
- 28 L. Xiong, H. Yu, G. Yang, M. Qiu, J. Chen and Y. Yu, *Thin Solid Films*, 2010, 518, 6738.
- 29 W. W. Yu and X. G. Peng, *Angew. Chem. Int. Ed.*, 2002, 41, 2368.
- 30 K. P. Musselman, A. Marin, A. Wisnet, C. Scheu, J. L. MacManus-Driscoll and L. Schmidt-Mende, *Adv. Funct. Mater.*, 2011, 21, 573.
- 31 F. Fabregat-Santiago, J. Bisquert, G. Garcia-Belmonte, G. Boschloo and A. Hagfeldt, *Sol. Energ. Mater. Sol. C.*, 2005, 87, 117.
- 32 B.-L. He, B. Dong and H.-L. Li, *Electrochem. Commun.*, 2007, 9, 425.
- 33 J. W. Ondersma and T. W. Hamann, *J. Phys. Chem. C*, 2010, 114, 638.
- 34 H.-J. Kim, D.-J. Kim, S. S. Rao, A. D. Savariraj, K. Soo-Kyoung, M.-K. Son, C. V. V. M. Gopi and K. Prabakar, *Electrochim. Acta*, 2014, 127, 427.
- 35 R. Zhou, Q. Zhang, E. Uchaker, L. Yang, N. Yin, Y. Chen, M. Yin and G. Cao, *Electrochim. Acta*, 2014, 135, 284.
- 36 I. Zarazua, T. Lopez-Luke, J. Reyes-Gomez, A. Torres-Castro, J. Z. Zhang and E. De la Rosa, *J. Electrochem. Soc.*, 2013, 161, H68.
- 37 I. Mora-Sero, S. Gimenez, F. Fabregat-Santiago, R. Gomez, Q. Shen, T. Toyoda and J. Bisquert, *Acc Chem Res*, 2009, 42, 1848.
- 38 G. Hodes, *J. Phys. Chem. C*, 2008, 112, 17778.
- 39 L. k. Tsui, L. Wu, N. Swami and G. Zangari, *ECS Electrochem. Lett.*, 2012, 1, D15.
- 40 A. Paracchino, V. Laporte, K. Sivula, M. Gratzel and E. Thimsen, *Nat. Mater.*, 2011, 10, 456.
- 41 Z. Zhang and P. Wang, *J. Mater. Chem.*, 2012, 22, 2456.
- 42 P. Wang, Y. H. Ng and R. Amal, *Nanoscale*, 2013, 5, 2952.
- 43 M. Yin, C. K. Wu, Y. Lou, C. Burda, J. T. Koberstein, Y. Zhu and S. O'Brien, *J. Am. Chem. Soc.*, 2005, 127, 9506.